Multidrug Resistance-Associated Protein–Overexpressing Teniposide-Resistant Human Lymphomas Undergo Apoptosis by a Tubulin-Binding Agent

Ritu Aneja,[1] Min Liu,[2] Clayton Yates,[3] Jinmin Gao,[2] Xin Dong,[2] Binfei Zhou,[1] Surya N. Vangapandu,[1] Jun Zhou,[2] and Harish C. Joshi[1]

[1]Department of Cell Biology, Emory University School of Medicine, Atlanta, Georgia; [2]Department of Genetics and Cell Biology, College of Life Sciences, Nankai University, Tianjin, China; and [3]Department of Biology and Center for Cancer Research, Tuskegee University, Tuskegee, Alabama

Abstract

Several DNA- and microtubule-binding agents are used to manage hematologic malignancies in the clinic. However, drug resistance has been a challenge, perhaps due to a few surviving cancer stem cells. Toxicity is another major impediment to successful chemotherapy, leading to an impoverished quality of life. Here, we show that a semisynthetic nontoxic tubulin-binding agent, 9-bromonoscapine (EM011), effectively inhibits growth and regresses multidrug resistance-associated protein (MRP)-overexpressing teniposide-resistant T-cell lymphoma xenografts and prolongs longevity. As expected, teniposide treatment failed to regress teniposide-resistant xenografts, rather, treated mice suffered tremendous body weight loss. Mechanistically, EM011 displays significant antiproliferative activity, perturbs cell cycle progression by arresting mitosis, and induces apoptosis in teniposide-resistant lymphoblastoid T cells both *in vitro* and *in vivo*. EM011-induced apoptosis has a mitochondrially-mediated component, which was attenuated by pretreatment with cyclosporin A. We also observed alterations of apoptosis-regulatory molecules such as inactivation of Bcl2, translocation of BAX to the mitochondrial membrane, cytochrome *c* release, and activation of downstream apoptotic signaling. EM011 caused DNA degradation as evident by terminal deoxynucleotidyl transferase–mediated dUTP-biotin end labeling staining of the increased concentration of 3′-DNA ends. Furthermore, the apoptotic induction was caspase dependent as shown by cleavage of the caspase substrate, poly(ADP)ribose polymerase. In addition, EM011 treatment caused a suppression of natural survival pathways such as the phosphatidylinositol-3′-kinase/Akt signaling. These preclinical findings suggest that EM011 is an excellent candidate for clinical evaluation. [Cancer Res 2008;68(5):1495–503]

Introduction

It is estimated that in the United States, every 10 minutes, a patient dies from blood cancer. Among the currently available treatment strategies (chemotherapy, radiation therapy, and bone marrow transplantation), chemotherapy, by far, is the largest subset of treatment options; and various classes of drugs including epipodophyllotoxins (etoposide and teniposide) and *Vinca alkaloids* (vinblastine and vincristine) are used to manage hematologic malignancies (1–3). Although the initial response to these drugs is impressive, their potential is limited by the development of multidrug resistance (4, 5), primarily mediated by overexpression of transmembrane efflux pumps [for example, the M_r 170,000 dalton P-glycoprotein (pgp) and the multidrug resistance-associated protein (MRP)] that reduce intracellular drug concentrations to suboptimal levels, thus, hindering clinical applicability (6, 7). Another major challenge is toxicity of currently available drug regimens that includes gastrointestinal toxicity, myelosuppression, immunosuppression, neurotoxicity, and alopecia (8, 9). Furthermore, because most of these drugs are administered i.v., multiple infections and frequent hospital visits cannot be avoided (10, 11). Thus, there is an urgent need to develop novel drugs that are efficacious, well-tolerated, nontoxic, orally available, can overcome various modes of resistance to conventional chemotherapeutics, and display better pharmacologic profiles.

Our laboratory has discovered a previously unknown tubulin-binding anticancer property (12–18) of a natural, nontoxic, orally available compound, noscapine, which is widely used as a cough suppressant in many countries including Western Europe, South America, and Asia. After our work, noscapine is already in phase I/II clinical trials for Non-Hodgkin's Lymphoma or Chronic Lymphocytic Leukemia refractory to chemotherapy. Our continued efforts to chemically synthesize novel noscapinoids based on modifications of the parent noscapine and to evaluate their biological activities for further drug development led to the identification of 9-bromonoscapine (EM011), a significantly more potent tubulin-binding anticancer agent than noscapine (19, 20), which preserves the nontoxic attributes of noscapine.

Although epipodophyllotoxins, such as teniposide and etoposide, are widely used to manage hematologic malignancies, prolonged teniposide therapy results in the development of drug resistance (21). Our laboratory has shown that EM011 regresses pgp-overexpressing human lymphoma xenografts implanted in nude mice (22). We were thus inquisitive to examine if tumors that exhibit drug-resistant phenotype due to other mechanisms, such as MRP overexpression (as in teniposide-resistant lymphomas), respond to EM011 therapy. This also offered us an opportunity to investigate if EM011 is efficacious in tumors that have become resistant to other nontubulin-binding conventional agents, such as teniposide, actively used for lymphoma management. Our present *in vitro* findings suggest that EM011 shows significant antiproliferative and apoptotic activity that was preceded by a potent G_2-M arrest in teniposide-resistant (CEM/VM-1-5) human T-lymphoma cells. Our *in vivo* data show the effectiveness of oral EM011 therapy to regress

Requests for reprints: Harish C. Joshi or Ritu Aneja, Department of Cell Biology, Emory University School of Medicine, Atlanta, GA 30322. Phone: 404-727-0445; E-mail: joshi@cellbio.emory.edu or raneja@emory.edu.

doi:10.1158/0008-5472.CAN-07-1874

teniposide-resistant lymphoma xenografts implanted in athymic nude mice. Importantly, unlike teniposide, EM011 is unique in being nontoxic to tissues with frequently dividing cells such as the gut and spleen. We therefore believe that EM011 is an ideal chemotherapeutic agent that merits a thorough clinical evaluation.

Materials and Methods

Reagents and cell culture. EM011 was prepared as described previously (19). Primary antibodies against human proteins [cytochrome *c*, caspase-3, poly(ADP-ribose) polymerase (PARP), phosphorylated Akt (p-Akt), Akt, phosphorylated BubR1, glyceraldehyde-3-phosphate dehydrogenase, and Bim] were from Cell Signaling. The human β-actin antibody was from Santa Cruz. All secondary antibodies were from Jackson ImmunoResearch. Monoclonal antibody for α-tubulin and cyclosporin A was from Sigma. Cell culture reagents were from Mediatech, Cellgro. CEM, a human lymphoblastoid line and its drug-resistant variant, CEM/VM-1-5, were grown in RPMI 1640 supplemented with 10% fetal bovine serum (Invitrogen) and 1% penicillin/streptomycin. Adenoviruses encoding β-galactosidase, dominant-negative BubR1, and dominant-negative Bim were prepared and amplified in low-passage human embryonic kidney 293 cells as described previously (23, 24).

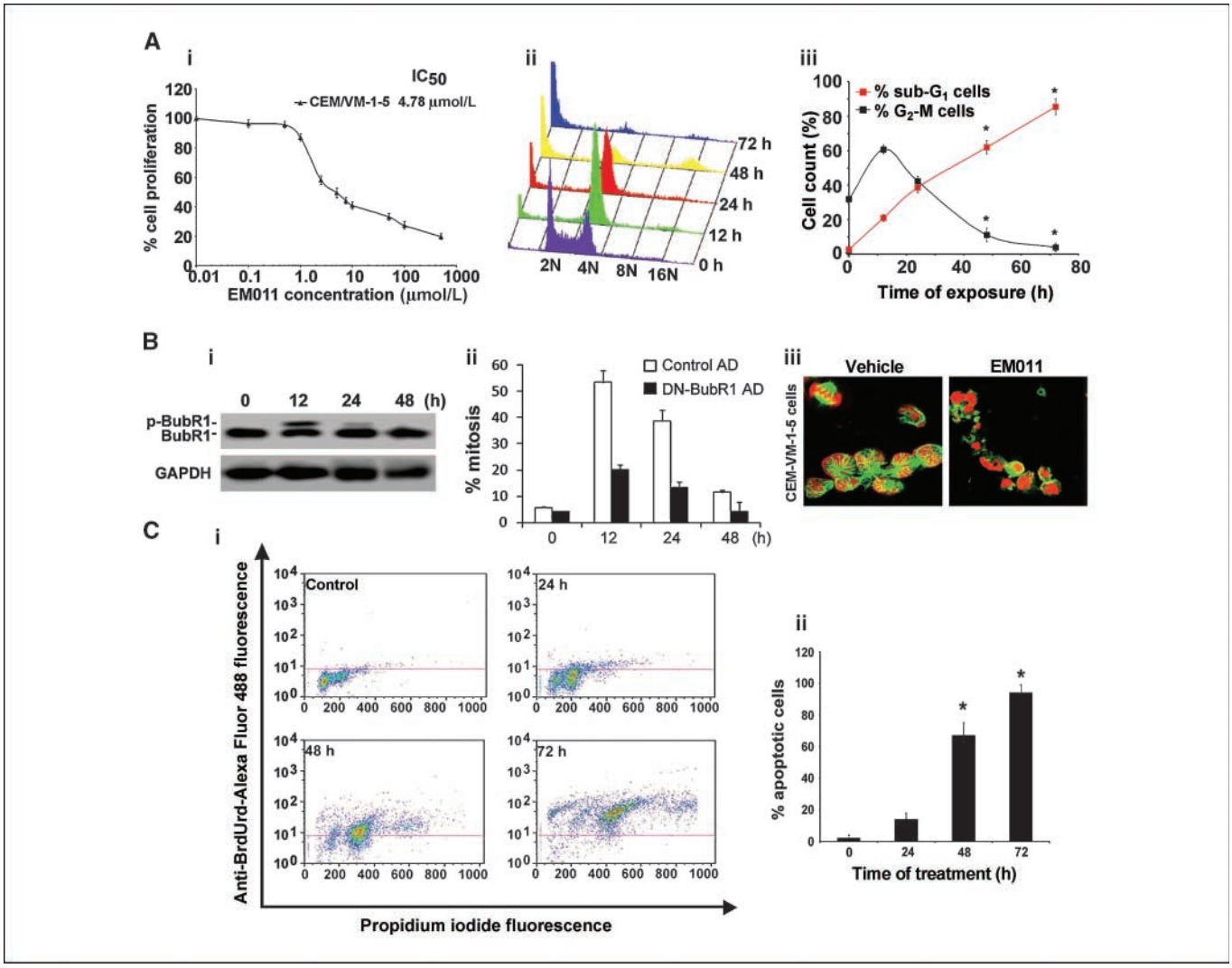

Figure 1. EM011 inhibits cell proliferation, arrests mitosis by activation of the spindle checkpoint, and induces apoptosis in teniposide-resistant human lymphoma cells. *Ai,* a plot of percent cell survival versus EM011 concentrations used for the determination of IC_{50} value (drug concentration needed to prevent cell proliferation by 50%). *Aii,* the cell cycle profile as a function of time of treatment in a three-dimensional disposition in CEM/VM-1-5 cells, as determined by FACS analyses. *x-axis*, DNA content of the cells; *y-axis*, number of cells detected for a given DNA content; *z-axis*, time of treatment. *2N,* cells residing in the G_0-G_1 phase of the cell cycle; *4N,* cells in the G_2 phase or in mitosis; *8N or 16N,* polyploid populations. *Aiii,* the percentage of G_2-M and sub-G_1 cells (indicative of degraded DNA) as a function of time of treatment (*, $P < 0.05$). *Bi,* EM011 treatment triggers spindle checkpoint activation as demonstrated by the phosphorylation of BubR1. *Bii,* impairment of the spindle checkpoint by dominant-negative (*DN*) BubR1 adenoviruses inhibits the activity of EM011 to arrest mitosis. β-galactosidase adenoviruses were used as control. *Biii,* confocal micrographs of vehicle-treated cells show intricate microtubule arrays (*left*) and mitoses (*top left, inset*). Ten micromoles of EM011 treatment completely changes the morphology by fragmentation of condensed chromatin in CEM/VM-1-5 cells (*right*). Images were obtained using a 63× objective with a numerical aperture of 1.4. *Ci,* CEM/VM-1-5 cells show extensive apoptosis as determined by a flow-cytometry–based TUNEL assay. Cells were treated with 10 μmol/L EM011 for 0, 24, 48, and 72 h. After the indicated incubation times, cells were processed for a flow cytometry–based terminal deoxynucleotidyl transferase (TdT)_mediated bromo_deoxyuridine triphosphate (BrdUTP) reaction. Addition of BrdUTP to the TdT reaction provides a means to label the DNA strand breaks and is detected by an Alexa Fluor 488–labeled anti-BrdUrd antibody. DNA content was determined by the binding of DNA-specific dye, propidium iodide (*x-axis*). Apoptotic cells were determined by incorporation of BrdUrd at the 3′-OH ends of the fragmented DNA as measured by anti-BrdUrd Alexa Fluor 488 fluorescence (*y-axis*). Data shown are from a representative experiment of three experiments performed. *Cii,* the quantitation of apoptotic cells indicated by the number of Alexa Fluor 488–positive cells of the total gated cells (*, $P < 0.05$).

Table 1. Effect of EM011 on cell cycle progression of CEM/VM-1-5 cells

Cell cycle variables, %	CEM/VM-1-5				
	0 h	12 h	24 h	48 h	72 h
G_0-G_1	33.0 ± 3.6	2.2 ± 0.5	2.2 ± 0.4	1.9 ± 0.2	1.4 ± 0.3
S	22.1 ± 1.8	6.0 ± 0.2	4.8 ± 0.4	3.7 ± 0.4	2.0 ± 0.3
G_2-M	31.9 ± 2.8	60.7 ± 3.6	42.2 ± 4.1	11.1 ± 0.8	3.9 ± 0.6
Sub-G_1	2.6 ± 0.3	20.9 ± 1.2	38.6 ± 3.2	62.0 ± 4.8	85.5 ± 5.6
Polyploid	10.8 ± 0.5	10.4 ± 0.9	12.6 ± 1.1	21.5 ± 2.2	7.4 ± 0.6

NOTE: Values shown are mean ± SE. $P < 0.05$.

Growth inhibition 3-(4,5-dimethylthiazol-2-yl)-5-(3-carboxymethoxyphenyl)-2-(4-sulfophenyl)-2H-tetrazolium, inner salt assay. Cells at a density of 5,000 cells/mL per well in a 96-well format were exposed to various EM011 concentrations for 48 h, and cell proliferation was measured colorimetrically by 3-(4,5-dimethylthiazol-2-yl)-5-(3-carboxymethoxyphenyl)-2-(4- sulfophenyl)-2H-tetrazolium, inner salt assay, using the CellTiter96 AQueous One Solution Reagent (Promega).

Analysis of cell cycle distribution and immunocytochemistry. The flow cytometric evaluation of the cell cycle status was performed as described previously (22). Briefly, 10 μmol/L EM011-treated cells were fixed in 70% ethanol, stained with propidium iodide and RNase A, followed by analyses on a FACSCalibur flow cytometer (Becton Dickinson). Immunofluorescence confocal microscopy was performed as previously described (22).

Evaluation of the mitochondrial transmembrane potential. The ampholytic cationic fluorescent probe dihexylocarbocyanine iodide [DiOC6(3)] was used to monitor EM011-induced changes in the mitochondrial transmembrane potential. After drug incubations, cells were loaded with 50 nmol/L of the probe DiOC6(3) for 30 min at 37°C. The supernatant was removed, and the cells were harvested and resuspended in PBS. The measurement of retained DiOC6(3) was examined flow cytometrically.

Immunoblot analysis. Proteins were resolved by SDS-PAGE and transferred onto polyvinylidene difluoride membranes (Millipore) that were blocked and incubated with primary and horseradish peroxidase (HRP)-conjugated secondary antibodies for 2 h and 1 h, respectively. Specific proteins were visualized with enhanced chemiluminescence detection reagent according to the manufacturer's instructions (Pierce Biotechnology). For cytochrome *c* release assays, cells were lysed in lysis buffer [10 mmol/L HEPES (*N*-2-hydroxyethylpiperazine-*N*′-2-ethanesulfonic acid; pH 7.5), 10 mmol/L KCl, and 1 mmol/L EDTA] with protease inhibitor cocktail (Sigma), frozen and thawed thrice, and spun at 2,000 × *g* for 5 min; and the supernatant was further centrifuged at 60,000 × *g* for 30 min at 4°C. The supernatant was analyzed for cytochrome *c* content by immunoblotting. β-actin was used as a loading control. All Western blot experiments were repeated at least twice with similar results.

Preparation of microtubule and supernatant fractions of cell extracts. The microtubule and supernatant fractions of cell extracts were prepared as described previously (23). Briefly, cells were treated with 10 μmol/L EM011 for the noted hours, washed, and soluble proteins were then extracted under conditions that prevent microtubule depolymerization [0.1% Triton X-100, 0.1 mol/L MES (pH 6.75), 1 mmol/L $MgSO_4$, 2 mmol/L EGTA, and 4 mol/L glycerol]. The remaining microtubule fraction was dissolved in 0.5% SDS in 25 mmol/L Tris (pH 6.8). Total protein concentration was then determined in each fraction, and equivalent amounts for each treatment group were loaded on the gel.

Determination of caspase-3 activity and terminal deoxynucleotidyl-transferase–mediated dUTP nick-end labeling assay for apoptosis. Caspase-3 activity was measured using the CaspaseGlo 3/7 Assay System kit (Promega Corporation) as described previously (22). DNA strand breaks were identified by using the terminal deoxynucleotidyl-transferase–mediated dUTP nick-end labeling (TUNEL) assay as previously described (22). Confocal micrographs were also obtained for the TUNEL-stained cells using a ×63 objective.

Animals and implantation of cancer cells. Eight- to ten-week-old female BALB/c athymic (nu/nu) nude mice (Harlan-Sprague Labs) were housed in the Emory University Animal Care Facility and were injected s.c. with 10^6 CEM/VM-1-5 cells per mouse. Treatment was initiated 7 to 10 days later when tumors were palpable and measurable (~100 mm^3). In control vehicle-treated groups of each experiment, the rapidly growing lymphoma tumors required that animals be euthanized when tumor volumes were ≥4,000 mm^3 or became ulcerated and the mice showed morbidity [Institutional Animal Care and Use Committee (IACUC) guidelines of Emory University]. This served as an end point for these experiments. For survival studies, the treated groups were observed for 120 days before euthanasia.

Drug treatment. Tumor-bearing mice were randomly grouped (eight mice per group). One group of mice were given EM011 (300 mg/kg) in deionized water (pH 4.0) by daily gavage. Untreated mice received equal volumes of deionized water (pH 4.0) only. Another group of mice were treated with 20 mg/kg teniposide (thrice a week) i.v., and untreated control animals received the vehicle solution i.v. Body weight was monitored every consecutive day.

Histopathologic and immunohistochemical analyses. At the end point of control and treatment groups (38 and 120 days, respectively), spleen, small intestines, liver, and regressed tumors were formalin fixed, paraffin embedded; and 5-μm sections were stained with H&E. TUNEL staining of tumor tissue sections was performed as previously described (22). Activated caspase-3 and Ki67 were detected by immunostaining tumor sections using specific monoclonal antibodies (DAKO) followed by HRP-coupled anti-mouse IgG staining. Cleaved PARP and phospho-H3 were detected by immunostaining using a specific monoclonal antibody (Cell Signaling) followed by HRP-coupled anti-rabbit IgG staining. Counter staining was done using hematoxylin.

Statistical analysis. The mean and SE were calculated for all quantitative experiments using Microsoft Excel software. The Student's *t* test was used to determine statistically significant differences between groups. *P* values of <0.05 were considered statistically significant.

Results and Discussion

EM011 Inhibits Cell Proliferation and Arrests Teniposide-Resistant Human Lymphoma Cells at Mitosis by Activation of the Spindle Checkpoint

The teniposide-resistant T-lymphoma cells, CEM/VM-1-5, show profound resistance to teniposide (~400-fold), owing to MRP overexpression, compared with parental CEM cells (25). To examine whether these cells respond to EM011, we first evaluated

the effect of EM011 on cellular proliferation. We found that the IC_{50} of EM011 for these cells was 4.78 μmol/L (Fig. 1*Ai*). Because EM011 is a tubulin-binding agent that blocks mitosis (22, 26), our next aim was to follow the cell cycle progression of CEM/VM-1-5 cells upon drug treatment over time. EM011 treatment resulted in a time-dependent accumulation of cells in the G_2-M phase as revealed by an increasing population of cells with 4N DNA with concomitant losses from G_0-G_1 phases (Table 1). Figure 1*Aii* displays the three-dimensional profile of cell cycle progression versus time of treatment. Our results show that the G_2-M arrest maximized (~61%) at 12 h of treatment (Fig. 1*Diii*). After this, we observed a disappearance of the G_2-M population and emergence of a characteristic hypodiploid (<2N DNA) sub-G_1 peak, indicating apoptotic cells (Fig. 1*Aii* and *Aiii*). This apoptotic population peaked at 72 h (~86%; Fig. 1*Aiii*) posttreatment. Together, these *in vitro* findings strongly indicate that EM011-treated cells arrest in the G_2-M phase before commencement of cell death.

We then investigated the molecular mechanisms underlying EM011-induced G_2-M arrest to understand its antiproliferative activity. Microtubule-binding agents such as paclitaxel and nocodazole are known to block cell cycle progression at mitosis by activation of the spindle checkpoint, a cellular surveillance mechanism that ensures accurate chromosome segregation (27). To examine whether EM011 arrests mitosis by triggering the spindle checkpoint, we analyzed the phosphorylation of BubR1, a component of the spindle checkpoint pathway that is phosphorylated during spindle checkpoint activation (28). As shown in Fig. 1*Bi*, EM011 treatment rapidly increased BubR1 phosphorylation level, indicating activation of spindle checkpoint. Importantly, impairment of the spindle checkpoint by dominant-negative BubR1 adenoviruses remarkably inhibited EM011-induced mitotic arrest (Fig. 1*Bii*). These data suggest a critical role for spindle checkpoint activation in mediating the early antiproliferative activity of EM011.

EM011 Triggers Apoptosis in Teniposide-Resistant Lymphoma Cells

Our next goal was to examine if EM011-induced cell death was due to apoptosis. Because apoptosis can be detected by characteristic changes in cellular morphology such as the disruption of cytoskeleton, membrane blebbing, hypercondensation and fragmentation of chromatin, and appearance of apoptotic bodies, we first microscopically visualized cells treated with EM011 for 72 h and compared them with vehicle-treated controls. Cells were stained using a α-tubulin–specific antibody (*green*) and a DNA-binding dye (*red*). The vehicle-treated cells showed intact normal radial microtubule arrays [Fig. 1*Biii, left*; *inset*, (*top left*)] shows a normal mitotic cell], whereas drug-treated cells showed perturbed microtubule arrays and fragmented DNA pieces (Fig. 1*Biii, right*). We also quantified the increase in concentration of 3-DNA ends due to DNA fragmentation upon EM011 treatment using a flow

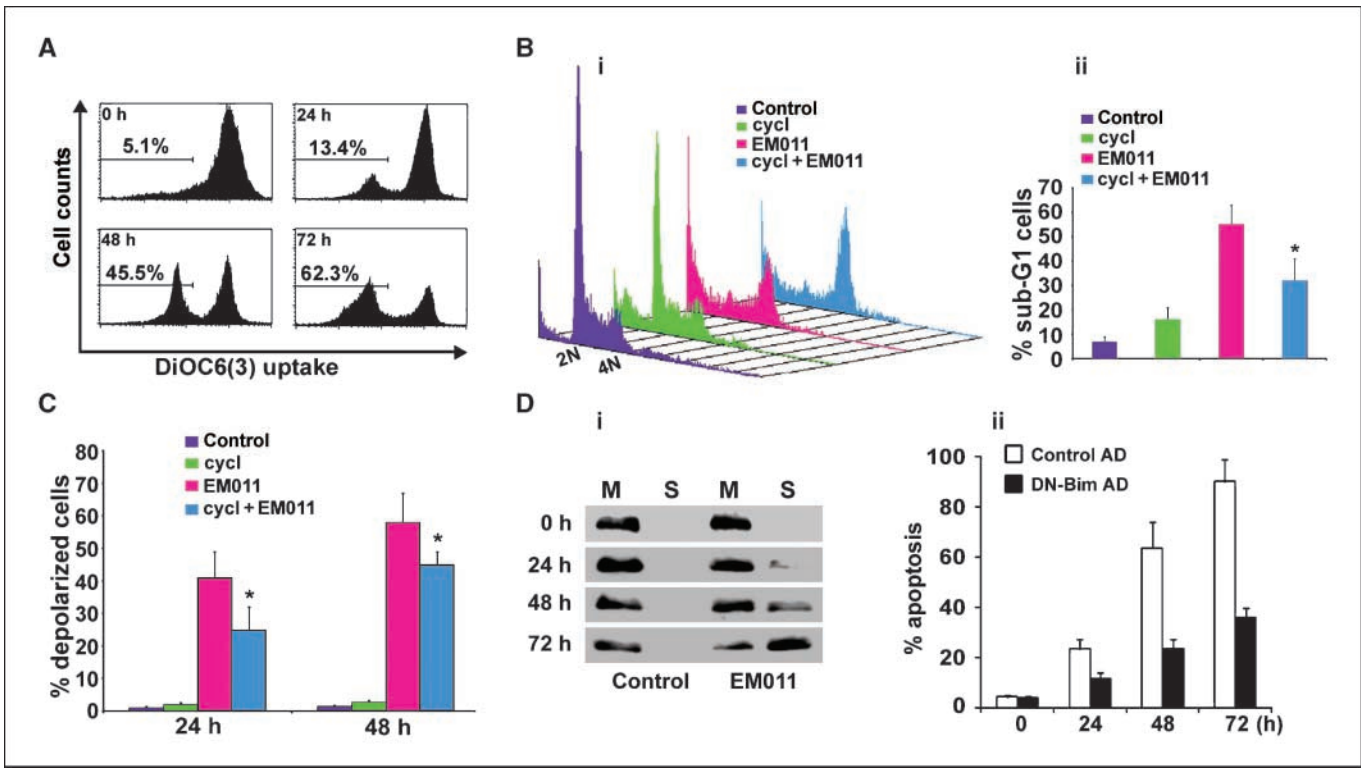

Figure 2. EM011-induced apoptosis has a mitochondrial component. *A,* EM011 treatment causes dissipation of mitochondrial transmembrane potential. Cells were treated with EM011 for 0, 24, 48 and 72 h followed by incubation with 50 nmol/L of DiOC6(3) and examined by flow cytometric analysis. *x-axis*, DiOC6(3) fluorescence intensity; *y-axis*, number of cells. Results are representative of three experiments performed. *B,* cyclosporin A pretreatment attenuates EM011-induced apoptosis. *Bi,* cells were pretreated with cyclosporin A for 3 h before subjection to EM011 treatment for 48 h, and the apoptotic sub-G_1 population was quantified flow cytometrically. Cell cycle profile of cells treated with DMSO (*control*), 10 μmol/L cyclosporin A, 10 μmol/L EM011, and cyclosporin A+EM011, for 48 h. *Bii,* quantitation of apoptotic cells (sub-G_1 population) upon these various treatments (*, $P < 0.05$). *C,* cyclosporin A pretreatment before EM011 exposure causes attenuations in the drop of mitochondrial transmembrane potential. Quantitation of number of depolarized cells upon various treatments. The decrease in the number of depolarized cells upon EM011/cyclosporin A cotreatment is significant compared with the number of depolarized cells upon EM011 treatment alone (*, $P < 0.05$). *D,* EM011 treatment causes Bim release from microtubules. *Di,* microtubule (*M*) and supernatant (*S*) fractions, respectively, of the cell extracts. *Dii,* dominant-negative (*DN*) Bim adenoviruses inhibit EM011-induced apoptosis. β-galactosidase adenoviruses were used as control.

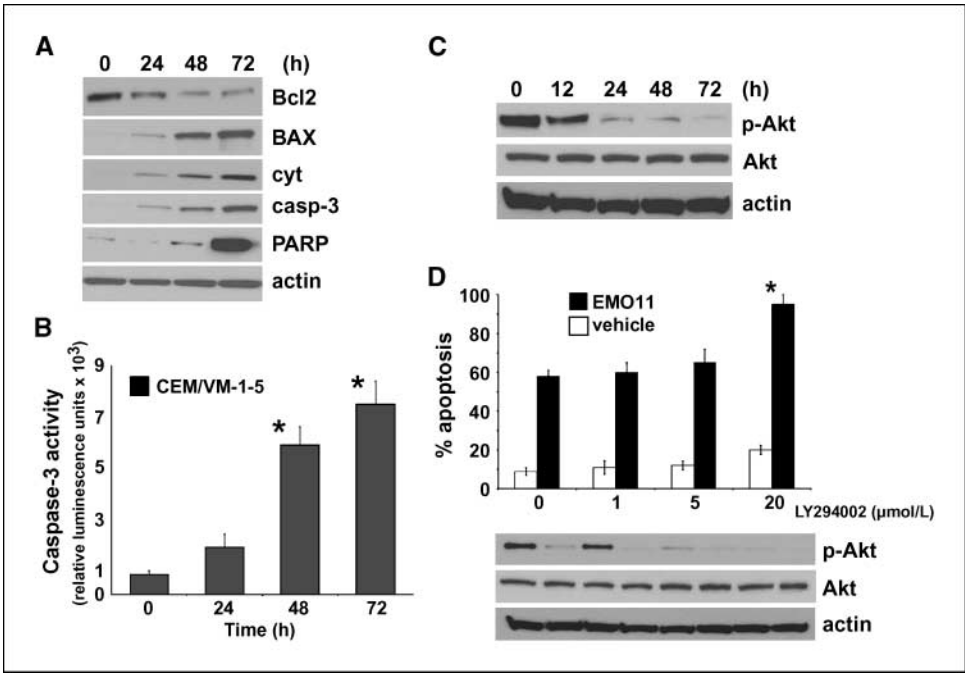

Figure 3. *A,* Western blot analysis of Bcl2, BAX, cytosolic cytochrome c, activated caspase-3, and cleaved PARP upon treatment of cells with EM011 for the indicated times. β-actin was used as a loading control. *B,* quantitation of time-dependent increase in caspase-3 activity upon EM011 treatment. Cells were treated with 10 μmol/L EM011 for 0, 24, 48, and 72 h; caspase-3 activity was analyzed using the luminogenic substrate Z-DEVD-aminoluciferin (*, $P < 0.05$). *C,* EM011 treatment causes Akt dephosphorylation. Representative immunoblots of p-Akt and total Akt protein levels upon EM011 treatment for the noted hours along with loading control, β-actin. *D,* EM011-induced apoptosis is augmented by inhibition of the PI3K/Akt pathway using LY294002, a specific PI3K inhibitor. Panel shows a bar-graphical representation of the percentage of apoptosis in cells treated for 48 h with 10 μmol/L EM011 or vehicle in the presence of 0, 1, 5, or 20 μmol/L LY294002 (*, $P < 0.05$). The level of Akt phosphorylation was examined by Western blot analysis.

cytometry–based TUNEL assay (Fig. 1*Ci*). Our results showed a time-dependent increase with ~67% TUNEL-positive cells at 48 h of treatment that peaked to ~94% at 72 h compared with vehicle-treated control cells (~2% TUNEL-positive cells; Fig. 1*Cii*).

EM011-Induced Apoptosis Has Mitochondrial Contributions

Loss of mitochondrial transmembrane potential. We next sought to investigate the mechanism of EM011-induced apoptosis. Among the various apoptotic pathways recruited by cells for their own demise, one major mechanism involves loss of mitochondrial membrane integrity and transmembrane potential (i.e., loss of $\Delta\Psi$m; ref. 29). This collapse of $\Delta\Psi$m is associated with inactivation of the antiapoptotic molecule Bcl2 and recruitment of BAX onto the outer mitochondrial membrane that results in uncoupling of the respiratory chain and efflux of small proapoptotic factors, eventually leading to activation of key executioner caspases, caspase-3/7 (30, 31). Because biochemical events, such as release of cytochrome *c* from mitochondria into the cytosol, caspase activation, and PARP cleavage, occur during the mitochondria-mediated apoptotic cell death (30, 31), we asked whether EM011-induced cell death was also accompanied by these biochemical events. Interestingly, we found a substantial time-dependent reduction in cellular uptake of fluorochrome DiOC6(3), indicating a loss of $\Delta\Psi$m when CEM/VM-1-5 cells were treated with 10 μmol/L EM011 (Fig. 2*A*). The percentage of depolarized cells increased as a function of time reaching a maximum of ~62% at 72 h (Fig. 2*A*). Although we can clearly see significant beginnings (~45%) of loss of $\Delta\Psi$m at 48 h, completely and directly mitochondrially-dependent apoptotic processes are kinetically much faster (32). These apoptotic processes (e.g., those induced by rotenone and atractyloside, mitochondrial respiratory chain inhibitors) are very rapid (15–20 min; ref. 32). However, this is contrary to what we observed in our studies with EM011 treatment, thus, pointing to additional or indirect effects of EM011 on the intrinsic mitochondrial pathway that were investigated next.

To address the extent of contribution of the mitochondrial pathway toward EM011-induced apoptosis, we used cyclosporin A, a mitochondrial permeability transition pore inhibitor. Our results show that pretreatment of cells with cyclosporin A for 3 h before EM011 treatment for 48 h resulted in ~39% sub-G_1 population compared with ~55% upon EM011 treatment alone (Fig. 2*Bi* and *Bii*). Our experiments to study the drop in $\Delta\Psi$m correlated with our flow cytometry data, in that we observed a diminution of number of cells with depolarized mitochondria when cyclosporin A was given 3 h before EM011 treatment compared with when EM011 was given alone (Fig. 2*C*). This is clearly indicative of the protective effect of cyclosporin A. These results suggest that there is a mitochondrial component to the total apoptotic response of EM011, although a partial one. Because mitochondria and microtubules are intimately linked to each other within cells (33), we next wanted to better understand the mechanism of how the mitochondrial pathway mediates EM011-induced apoptosis.

Bim release from microtubules. Bim, a protein interacting with microtubules, has been suggested as a sensor of microtubule integrity. Many microtubule-binding agents have been reported to induce Bim dissociation from microtubules, which then leads to apoptosis by affecting on mitochondrial events (34, 35). To test whether EM011 uses a similar mechanism to transduce signals from its effect on microtubules to mitochondria-dependent apoptosis, we examined the level of Bim in microtubule and supernatant fractions in cells. As shown in Fig. 2*Di*, Bim was entirely in the microtubule fraction in vehicle-treated cells, whereas a significant portion of Bim was detected in the supernatant fraction in EM011-treated cells, indicating that Bim dissociated from microtubules upon EM011 treatment. Moreover, dominant-negative Bim adenoviruses could dramatically prevent EM011 to induce apoptosis (Fig. 2*Dii*). These results thus suggest that Bim is crucial for EM011 to induce apoptosis through the mitochondrial pathway.

Increase in BAX/Bcl2 ratio and release of cytochrome *c* into the cytosol. One of the main regulatory steps of apoptotic cell

death is controlled by the ratio of antiapoptotic and proapoptotic members of the Bcl2 family of proteins, which determines the susceptibility to apoptosis. Our results showed that EM011 treatment increases BAX levels in a time-dependent manner, whereas Bcl2 levels were decreased, which led to an overall increase in the proapoptotic/antiapoptotic BAX/Bcl2 ratio as a function of time of treatment (Fig. 3*A*). The cytochrome *c* release was clearly detectable at 48 h and peaked at 72 h of drug treatment in the cytosolic fraction (Fig. 3*A*).

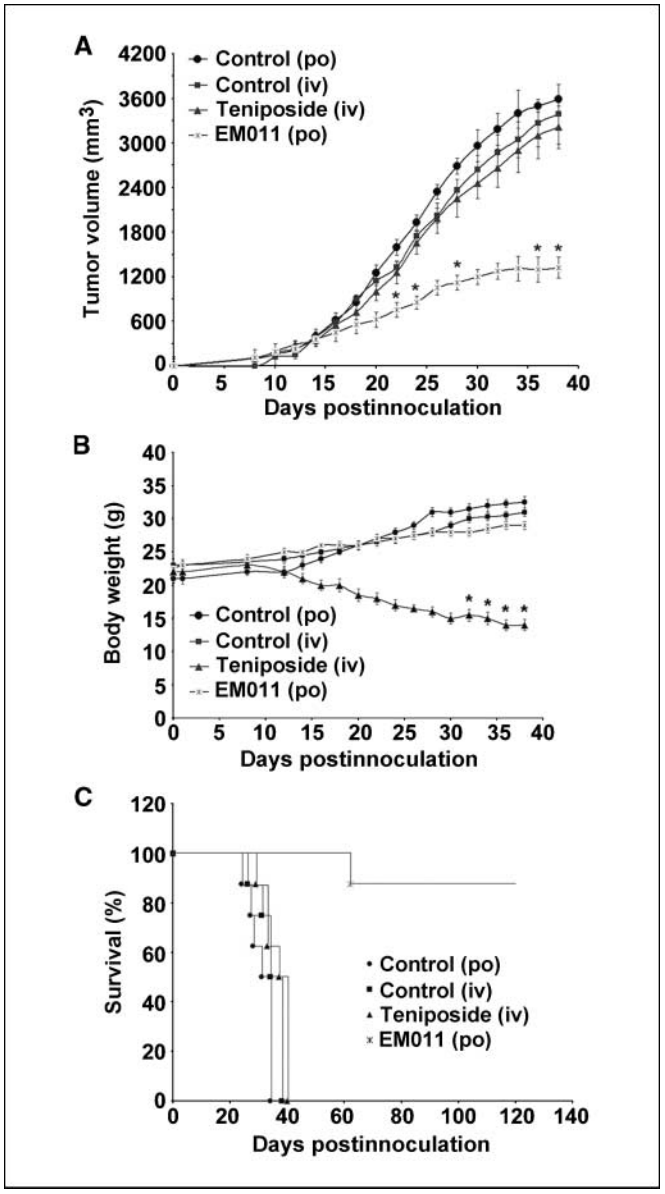

Figure 4. Daily oral treatment with 300 mg/kg body weight of EM011 significantly regresses teniposide-resistant T-cell lymphoma xenografts compared with matched controls. However, teniposide-resistant tumors fail to respond to teniposide therapy (20 mg/kg body weight administered intravenously thrice a week). *A,* a progression profile of tumor growth kinetics in EM011- and teniposide-treated animals compared with both orally and intravenously vehicle-treated matched controls, respectively. On day 38, control vehicle-treated mice were euthanized because of overgrown tumors, in compliance with experimental protocols approved by IACUC of Emory University. *Points,* mean of tumor volume shown as mm^3; *bars,* SE; *, $P < 0.05$. *B,* EM011 treatment was well-tolerated; mice did not suffer from body weight loss, whereas teniposide treatment significantly reduced body weight and caused morbidity ($P < 0.05$). *C,* EM011 confers a significant survival advantage over teniposide treatment compared with vehicle-treated matched controls over the 120-d study period as evident by Kaplan-Meier analysis.

Activation of executionery caspase, caspase-3, and cleavage of PARP. Our next aim was to examine the involvement of caspases that are activated upon cytochrome *c* release and play a major role in cleaving a variety of substrates. Because caspase-3 activation is considered as a hallmark of the apoptotic process, we monitored the active form of the cysteine protease using a small conserved modified peptide substrate that becomes luminogenic upon cleavage. As shown in Fig. 3*B*, EM011 stimulated a time-dependent increase of caspase-3 activity in CEM/VM-1-5 cells, and treatment of cells with a specific inhibitor of caspase-3 significantly blocked EM011-induced apoptotic cell death (data not shown). Our immunoblots also showed a time-dependent increase in the expression levels of activated caspase-3, suggesting that EM011-induced cell death is caspase-3 dependent (Fig. 3*A*). Once caspase-3 is activated, a number of cellular proteins are cleaved, including the PARP (36). Our results showed a time-dependent increase in cleaved PARP levels, a downstream substrate of the caspase cascade, and a reliable marker of apoptosis (Fig. 3*A*).

EM011 Treatment Causes Akt Dephosphorylation

One of the characteristics of cancer cells is their ability to evade programmed cell death through the activation of phosphatidylinositol 3-kinase (PI3K)/Akt pathway (37, 38). PI3K/Akt kinase activities have thus been shown to be elevated in primary tumors and cancer cell lines due to gene amplification, protein overexpression, or mutations of tumor suppressor genes (38). Activated Akt phosphorylates and inhibits proapoptotic proteins, including Bad, caspase-9, and forkhead transcription factors (39–42), thereby inhibiting apoptosis. Because PI3K/Akt constitutes an important cell survival pathway governing the apoptotic response, we next investigated the effect of EM011 on this pathway in a time course experiment. As the activity of Akt is regulated by phosphorylation, we examined the level of p-Akt Ser^{473} in CEM/VM-1-5 cells treated with EM011 at the noted time points (Fig. 3*C*). Our results showed a time-dependent decrease of p-Akt Ser^{473}, although total Akt protein levels remained unaffected (Fig. 3*C*). Because inhibition of PI3K/Akt pathway dramatically induces apoptosis in many cancer cell types, we investigated whether blocking the PI3K/Akt pathway altered the sensitivity of teniposide-resistant cells to EM011-induced apoptosis. Interestingly, our results showed that cotreatment of EM011 with 20 μmol/L LY294002, an inhibitor of PI3K, for 48 h, augmented EM011-induced apoptosis in CEM/VM-1-5 cells (Fig. 3*D*). In contrast, cotreatment with lower doses of the inhibitor (1 and 5 μmol/L) inhibited Akt phosphorylation; however, this did not result in significant differences in apoptotic cell death compared with EM011 alone, as indicated by percent sub-G_1 apoptotic population measured by fluorescence-activated cell sorting analysis (Fig. 3*D*). Because high dosages of LY294002 are proapoptotic and PI3K-independent in other cancer cell lines (43), it is likely that augmentation of EM011-induced apoptosis at 20 μmol/L LY294002 may be due to an interaction between LY294002 and EM011, which is not PI3K-dependent. Nonetheless, these experiments suggested that EM011 treatment causes suppression of the natural cell survival pathway. However, it is unlikely that inhibition of the PI3K/Akt pathway by EM011 plays a major role in the induction of apoptosis in these lymphoma cells.

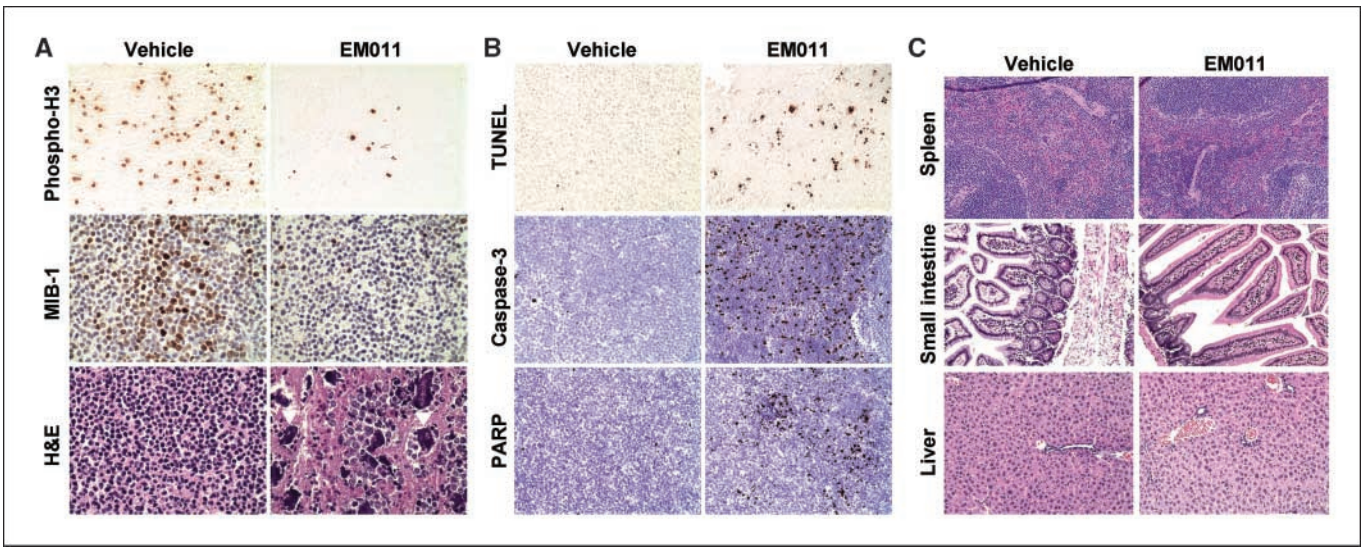

Figure 5. *A, in vivo* tumor reduction by EM011 is a result of remarkable antipoliferative and antimitotic activity of EM011. A widespread phosphorylated-histone H3 and MIB-1 staining (*top* and *middle, left*) in tumor sections from control vehicle-treated animals, whereas very little staining is seen in regressed tumor sections from EM011-treated animals (*top* and *middle, right*). Magnification, ×400. Tumors from both groups were excised at day 22 of treatment when significant regression was observable. *Bottom,* H&E staining of 5-μm histological sections of excised tumor tissue from animals treated with vehicle or EM011 for 22 d (when active tumor regression is evident). Cells with abnormal circular mitotic asters (*white arrowheads, bottom right*) were clearly visible as a result of EM011 treatment in the regressed tumors excised from drug-treated animals but were absent in tumor tissue from control vehicle-treated controls (*bottom left*). Magnification, ×400. *B,* EM011 induces apoptosis *in vivo*. Immunohistochemical staining of paraffin-embedded tumor sections for TUNEL staining as a hallmark of *in vivo* apoptosis from mice treated with the vehicle (*top left*) or EM011 (*top right*) for 38 d (end point of control vehicle-treated animals). *Right,* numerous TUNEL-positive cells (seen as apoptotic brown nuclei) compared with vehicle-treated control (*left*). EM011 induces caspase-3 and downstream PARP cleavage *in vivo*. Extensive activated caspase-3 and cleaved PARP staining in tumors excised at day 38 from EM011-treated groups (*middle* and *bottom, right*), as compared with vehicle-treated control groups (*middle* and *bottom, left*) is evident. *C,* daily 300-mg/kg EM011 treatment fails to reveal any detectable pathological abnormalities in normal tissues that are active in normal cell proliferation. Panels represent H&E staining of paraffin-embedded 5-μm thick sections of the spleen, gut, and liver from vehicle- and EM011-treated groups of mice visualized under ×400 magnification. There was no observable histopathological difference in these tissues between the two groups. The splenic follicles and vascular sinusoids were indistinguishable between the EM011- and vehicle-treated groups; the gut showed normal mucosa, submucosa, and muscularis mucosa. In addition, livers from animals of treatment group showed normal hepatic lobular architecture and intact portal tracts.

Oral EM011 Treatment Achieves Significant Tumor Volume Reduction of Teniposide-Resistant Xenografts in Athymic Nude Mice

Our laboratory has recently shown that EM011 effectively inhibits the growth of hormone-refractory breast tumors (26) and pgp-overexpressing vinblastine-resistant lymphomas implanted in nude mice (22). It was intriguing whether the anticancer effects of EM011 were restricted to tumors that are resistant due to overexpression of pgp drug efflux pumps or were applicable to other drug-resistant mechanisms such as overexpression of MRP. We also asked if tumors that are resistant to other widely used lymphoma drugs, such as teniposide, responded to EM011 therapy. Thus, to investigate the generality of the effectiveness of EM011, we evaluated its potential *in vivo* antitumor effects on teniposide-resistant T-cell lymphoma xenografts implanted in athymic nude mice. CEM/VM-1-5 cells were injected s.c. in nude mice, and 7 to 10 days after tumor implantation, when well-established xenografts were palpable with a tumor size of ~100 mm^3, mice were randomized into vehicle-control and treatment groups of eight animals each. The treatment groups received individually therapeutic dosages of EM011 (300 mg/kg orally, daily) and teniposide (20 mg/kg i.v., thrice a week). Because teniposide is clinically effective intravenously (unlike EM011, which is orally available), we included matched control groups receiving the vehicle solution orally as well as i.v. in our study. Tumor volumes were measured every consecutive day using vernier calipers. Mice were euthanized when tumors ulcerated or showed extreme morbid conditions, according to the IACUC regulations of Emory University. In vehicle-treated (both orally and i.v.) control animals, the tumors showed unrestricted progression (Fig. 4*A*). In clear contrast, oral EM011 treatment showed a time-dependent regression of tumor burden (Fig. 4*A*). A reduction in tumor burden by ~63% was observable at 38 days of oral administration. The difference between the mean final tumor volumes in animals receiving EM011 and those receiving vehicle solution orally was statistically significant ($P < 0.05$). All animals in the control group had to be euthanized by day 38 postinoculation due to tumor overburden, in compliance with the IACUC guidelines. Another treatment group examined the effect of i.v. teniposide administration on tumor volumes compared with their matched controls. As expected for teniposide-resistant xenografts, mice did not show any significant reduction in tumor volume upon 20 mg/kg i.v. teniposide treatment thrice a week compared with control animals (3,388 ± 400 mm^3 and 3,212 ± 289 cm^3, average tumor volume ± SE for vehicle- and teniposide-treated groups, respectively at day 38; Fig. 4*A*). No statistical differences were observed between tumor volumes in animals receiving teniposide or matched controls receiving the vehicle solution i.v. To assess the overall health and well-being of animals during drug treatment, we measured their body weight every consecutive day. As shown in Fig. 4*B*, mice in EM011 treatment group maintained normal weight gain and showed no signs of discomfort during the treatment regimen. Thus, EM011 treatment at a dose level of 300 mg/kg was well-tolerated and did not show any obvious adverse effect on the general health of treated mice. However, mice in the teniposide-treated group suffered significant body weight loss associated with morbidity (Fig. 4*B*). We next determined the longevity of surviving mice by monitoring them for general well-being for 120 days. Kaplan-Meier

analysis revealed a significantly increased survival time with 87.5% animals treated with EM011 surviving until day 120 ($P < 0.05$; Fig. 4*C*). This was a remarkable prolongation of survival compared with controls where the median survival time was only 31 days (Fig. 4*C*). The teniposide-treated animals did not survive beyond 40 days (Fig. 4*C*).

Our next question was to examine if tumor reduction upon EM011 therapy was also due to inhibition of cellular proliferation, mitotic arrest, and induction of apoptosis. Thus, to examine if the *in vivo* results were in congruence with *in vitro* data, we euthanized a subset of mice treated with EM011 orally for 22 days (when significant regression of tumor xenografts was observable) along with matched controls receiving the vehicle solution orally. The tumor tissue was excised followed by immunostaining of histologic sections for proliferation markers, such as the phosphorylated histone H3 and Ki67 antigen. The phospho-H3 antibody recognizes histone H3 after its phosphorylation on Ser^{10} upon chromosome condensation during prophase (44). A pronounced staining of phospho-H3 in control sections (Fig. 5*A, top left*) depicted rapidly proliferating cells, whereas a diminuted staining was observed in regressed tumor sections from EM011-treated mice (Fig. 5*A, top right*). Our data further showed that immunohistochemical staining with MIB-1, a monoclonal antibody against Ki67, resulted in a widespread expression of MIB-1–positive cells in control sections (Fig. 5*A, middle left*) reflecting aggressively proliferating cells, whereas only a few positive cells were visible in tumor sections derived from EM011-treated mice (Fig. 5*A, middle right*). These results suggested that EM011 inhibits *in vivo* cellular proliferation. We next asked if EM011 displayed similar antimitotic activity *in vivo* as well. Towards this goal, we H&E stained 5-μm tumor sections at day 22 of treatment. Circular mitotic figures (Fig. 5*A, bottom right, white arrowheads*) were clearly visible in the remaining regressed tumors excised from animals undergoing EM011 treatment but were absent in tumor tissue from vehicle-treated control animals (Fig. 5*A, bottom left*).

Our *in vitro* data showed that EM011 induced extensive apoptosis in teniposide-resistant cells. To draw parallel, we microscopically examined TUNEL-stained tumor sections from both vehicle-treated control and EM011-treated groups at 38 days (end point of control vehicle-treated animals). Consistent with our *in vitro* results from the TUNEL assay, we observed numerous TUNEL-positive cells (Fig. 5*B, top right*) in the regressed tumor sections of EM011-treated animals. We moved on to confirm if our *in vitro* findings indicating caspase-3 activation and PARP cleavage correlated with our *in vivo* results. Consistent with our *in vitro* data, we observed immunohistochemically a widespread expression of activated caspase-3 (Fig. 5*B, middle right*) and cleaved PARP (Fig. 5*B, bottom right*) in the small regressed tumor sections from mice of EM011-treatment group at day 38. In contrast, there was no significant staining in the control tumor sections (Fig. 5*B, middle* and *bottom left*). We thus concluded that the regression of tumor xenografts is a result of EM011-induced apoptosis.

EM011 Therapy Does Not Cause Any Histologic Toxicity

The rational approach of treating cancer is targeting of selective differences between a cancer cell and a normal host cell. Unfortunately, many of the available drugs do not discriminate very well between a normal and a neoplastic cell, rather target all rapidly dividing cells such as the gut and spleen. Thus, a range of unwanted toxic effects accompanies their use, which is a clear reflection of their nonselective behavior. Unlike conventional tubulin-binding chemotherapeutics that mess up the microtubule system in extremity, noscapinoids are distinctive, perhaps because they do not alter the steady-state monomer/polymer ratio of tubulin. Thus normal cells, owing to robust cell cycle checkpoint controls, arrest until the drug is cleared out by metabolism/excretion, whereas cancer cells due to mutational lesions in their checkpoint mechanisms do not halt for a longer duration. They rather continue to traverse the cell cycle, thus, accumulating massive DNA amounts that trigger apoptosis owing to genotoxic stress (14). Thus, to investigate if EM011 results in toxicities to normal tissues, we examined tissue sections of the spleen, gut, and liver of tumor-bearing mice by H&E staining (Fig. 5*C*). Our results showed that EM011 therapy did not cause any detectable pathologic abnormalities in mice, and there was a complete absence of metastatic lesions in these organs.

Taken together, our data provide compelling evidence that EM011 is efficacious in inducing apoptosis and suppressing growth of MRP overexpressing cells. More importantly, EM011 is potently active in regressing tumors that have become resistant to teniposide, a drug actively used for lymphoma management in the clinic. In addition, EM011 therapy is oral and nontoxic, which is a unique edge over currently available chemotherapeutics. Therefore, we believe that EM011 is a promising nontoxic drug candidate with potential for management of hematologic drug-resistant malignancies.

Acknowledgments

Received 5/20/2007; revised 12/1/2007; accepted 1/3/2008.

Grant support: NIH grants CA-095317-01A2 (H.C. Joshi) and 3P20MD000195-05S1 (C. Yates).

The costs of publication of this article were defrayed in part by the payment of page charges. This article must therefore be hereby marked *advertisement* in accordance with 18 U.S.C. Section 1734 solely to indicate this fact.

We wish to thank Dr. William T. Beck for providing cell lines, and members of the Joshi laboratory for discussions. We thankfully acknowledge Dr. Meenakshi Gupta, pathologist for evaluating animal tissue sections in a blinded manner.

References

1. Kluin-Nelemans HC, Zagonel V, Anastasopoulou A, et al. Standard chemotherapy with or without high-dose chemotherapy for aggressive non-Hodgkin's lymphoma: randomized phase III EORTC study. J Natl Cancer Inst 2001;93:22–30.
2. Hiddemann W, Unterhalt M, Buske C, Sack H. Treatment of follicular follicle centre lymphomas: current status and future perspectives. J Intern Med Suppl 1997;740:55–62.
3. Smith MA, Rubinstein L, Ungerleider RS. Therapy-related acute myeloid leukemia following treatment with epipodophyllotoxins: estimating the risks. Med Pediatr Oncol 1994;23:86–98.
4. Szakacs G, Paterson JK, Ludwig JA, Booth-Genthe C, Gottesman MM. Targeting multidrug resistance in cancer. Nat Rev Drug Discov 2006;5:219–34.
5. Gottesman MM. Mechanisms of cancer drug resistance. Annu Rev Med 2002;53:615–27.
6. Polgar O, Bates SE. ABC transporters in the balance: is there a role in multidrug resistance? Biochem Soc Trans 2005;33:241–5.
7. Hegewisch-Becker S, Hossfeld DK. The MDR phenotype in hematologic malignancies: prognostic relevance and future perspectives. Ann Hematol 1996;72:105–17.
8. Rowinsky EK. The development and clinical utility of the taxane class of antimicrotubule chemotherapy agents. Annu Rev Med 1997;48:353–74.
9. Zhou J, Giannakakou P. Targeting microtubules for cancer chemotherapy. Curr Med Chem Anticancer Agents 2005;5:65–71.
10. Van Zuylen L, Verweij J, Sparreboom A. Role of formulation vehicles in taxane pharmacology. Invest New Drugs 2001;19:125–41.
11. Dorr RT. Pharmacology and toxicology of Cremophor EL. Ann Pharmacother 1994;28:S11–14.
12. Ye K, Ke Y, Keshava N, et al. Opium alkaloid noscapine is an antitumor agent that arrests metaphase

and induces apoptosis in dividing cells. Proc Natl Acad Sci U S A 1998;95:1601–6.
13. Ke Y, Ye K, Grossniklaus HE, Archer DR, Joshi HC, Kapp JA. Noscapine inhibits tumor growth with little toxicity to normal tissues or inhibition of immune responses. Cancer Immunol Immunother 2000;49:217–25.
14. Landen JW, Lang R, McMahon SJ, et al. Noscapine alters microtubule dynamics in living cells and inhibits the progression of melanoma. Cancer Res 2002;62:4109–14.
15. Zhou J, Panda D, Landen JW, Wilson L, Joshi HC. Minor alteration of microtubule dynamics causes loss of tension across kinetochore pairs and activates the spindle checkpoint. J Biol Chem 2002;277:17200–8.
16. Zhou J, Gupta K, Yao J, et al. Paclitaxel-resistant human ovarian cancer cells undergo c-Jun NH2-terminal kinase-mediated apoptosis in response to noscapine. J Biol Chem 2002;277:39777–85.
17. Landen JW, Hau V, Wang M, et al. Noscapine crosses the blood-brain barrier and inhibits glioblastoma growth. Clin Cancer Res 2004;10:5187–201.
18. Joshi HC, Zhou J. Noscapine and analogues as potential chemotherapeutic agents. Drug News Perspect 2000;13:543–6.
19. Zhou J, Gupta K, Aggarwal S, et al. Brominated derivatives of noscapine are potent microtubule-interfering agents that perturb mitosis and inhibit cell proliferation. Mol Pharmacol 2003;63:799–807.
20. Aneja R, Vangapandu SN, Lopus M, et al. Synthesis of microtubule-interfering halogenated noscapine analogs that perturb mitosis in cancer cells followed by cell death. Biochem Pharmacol 2006;72:415–26.
21. Bird MC, Bosanquet AG, Forskitt S, Gilby ED. Long-term comparison of results of a drug sensitivity assay *in vitro* with patient response in lymphatic neoplasms. Cancer 1988;61:1104–9.
22. Aneja R, Zhou J, Vangapandu SN, Zhou B, Chandra R, Joshi HC. Drug-resistant T-lymphoid tumors undergo apoptosis selectively in response to an antimicrotubule agent, EM011. Blood 2006;107:2486–92.
23. Liu M, Aneja R, Liu C, et al. Inhibition of the mitotic kinesin Eg5 up-regulates Hsp70 through the phosphatidylinositol 3-kinase/Akt pathway in multiple myeloma cells. J Biol Chem 2006;281:18090–7.
24. Xuan C, Qiao W, Gao J, et al. Regulation of microtubule assembly and stability by the transactivator of transcription protein of Jembrana disease virus. J Biol Chem 2007;282:28800–6.
25. Morgan SE, Kim R, Wang PC, et al. Differences in mutant p53 protein stability and functional activity in teniposide sensitive and -resistant human leukemic CEM cells compared with parental CEM cells. Oncogene 2000;19:5010–9.
26. Aneja R, Zhou J, Zhou B, Chandra R, Joshi HC. Treatment of hormone-refractory breast cancer: apoptosis and regression of human tumors implanted in mice. Mol Cancer Ther 2006;5:2366–77.
27. Zhou J, Yao J, Joshi HC. Attachment and tension in the spindle assembly checkpoint. J Cell Sci 2002;115:3547–55.
28. Li W, Lan Z, Wu H, et al. BUBR1 phosphorylation is regulated during mitotic checkpoint activation. Cell Growth Differ 1999;10:769–75.
29. Green DR, Reed JC. Mitochondria and apoptosis. Science 1998;281:1309–12.
30. Liu X, Kim CN, Yang J, Jemmerson R, Wang X. Induction of apoptotic program in cell-free extracts: requirement for dATP and cytochrome *c*. Cell 1996;86:147–57.
31. Li P, Nijhawan D, Budihardjo I, et al. Cytochrome *c* and dATP-dependent formation of Apaf-1/caspase-9 complex initiates an apoptotic protease cascade. Cell 1997;91:479–49.
32. Isenberg JS, Klaunig JE. Role of the mitochondrial membrane permeability transition (MPT) in rotenone-induced apoptosis in liver cells. Toxicol Sci 2000;53:340–51.
33. Ball EH, Singer SJ. Mitochondria are associated with microtubules and not with intermediate filaments in cultured fibroblasts. Proc Natl Acad Sci U S A 1982;79:123–6.
34. Puthalakath H, Huang DC, O'Reilly LA, King SM, Strasser A. The proapoptotic activity of the Bcl-2 family member Bim is regulated by interaction with the dynein motor complex. Mol Cell 1999;3:287–96.
35. Marani M, Tenev T, Hancock D, Downward J, Lemoine NR. Identification of novel isoforms of the BH3 domain protein Bim which directly activate Bax to trigger apoptosis. Mol Cell Biol 2002;22:3577–89.
36. Kaufmann SH, Desnoyers S, Ottaviano Y, Davidson NE, Poirier GG. Specific proteolytic cleavage of poly(-ADP-ribose) polymerase: an early marker of chemotherapy-induced apoptosis. Cancer Res 1993;53:3976–85.
37. Hanahan D, Weinberg RA. The hallmarks of cancer. Cell 2000;100:57–70.
38. Vivanco I, Sawyers CL. The phosphatidylinositol 3-Kinase AKT pathway in human cancer. Nat Rev Cancer 2002;2:489–501.
39. Khwaja A. Akt is more than just a Bad kinase. Nature 1999;401:33–4.
40. Datta SR, Dudek H, Tao X, et al. Akt phosphorylation of Bad couples survival signals to the cell-intrinsic death machinery. Cell 1997;91:231–41.
41. Brunet A, Bonni A, Zigmond MJ, et al. Akt promotes cell survival by phosphorylating and inhibiting a forkhead transcription factor. Cell 1999;98:857–66.
42. Cardone MH, Roy N, Stennicke HR, et al. Regulation of cell death protease caspase-9 by phosphorylation. Science 1998;282:1318–21.
43. Yang CC, Lin HP, Chen CS, et al. Bcl-xL mediates a survival mechanism independent of the phosphoinositide 3-kinase/Akt pathway in prostate cancer cells. J Biol Chem 2003;278:25872–8.
44. Strahl BD, Allis CD. The language of covalent histone modifications. Nature 2000;403:41–5.

Multidrug Resistance-Associated Protein–Overexpressing Teniposide-Resistant Human Lymphomas Undergo Apoptosis by a Tubulin-Binding Agent

Ritu Aneja, Min Liu, Clayton Yates, et al.

Cancer Res 2008;68:1495-1503.